Glycogen storage disease type III: A novel Agl knockout mouse model

Serena Pagliarani [a,1], Sabrina Lucchiari [a,1], Gianna Ulzi [a], Raffaella Violano [b], Michela Ripolone [b], Andreina Bordoni [a], Monica Nizzardo [a], Stefano Gatti [c], Stefania Corti [a], Maurizio Moggio [b], Nereo Bresolin [a], Giacomo P. Comi [a,]

[a] Dino Ferrari Center, Neuroscience Section, Department of Pathophysiology and Transplantation (DEPT), University of Milan, Neurology Unit, IRCCS Foundation Ca' Granda Ospedale Maggiore Policlinico, Milan, Italy
[b] Neuromuscular Unit — Fondazione I.R.C.C.S. Ca' Granda, Ospedale Maggiore Policlinico, Milano, Dino Ferrari Centre, University of Milan, Italy
[c] Center for Surgical Research, Fondazione IRCCS Ca' Granda, Ospedale Maggiore Policlinico, Milan, Italy

a b s t r a c t

Glycogen storage disease type III is an autosomal recessive disease characterized by a deficiency in the glycogen debranching enzyme, encoded by AGL. Essential features of this disease are hepatomegaly, hypoglycemia, hyperlipidemia, and growth retardation. Progressive skeletal myopathy, neuropathy, and/or cardiomyopathy become prominent in adults. Currently, there is no available cure. We generated an Agl knockout mouse model by deletion of the carboxy terminus of the protein, including the carboxy end of the glucosidase domain and the glycogen-binding domain. Agl knockout mice presented serious hepatomegaly, but we did not observe signs of cirrhosis or adenomas. In affected tissues, glycogen storage was higher than in wild-type mice, even in the central nervous system which has never been tested in GSDIII patients. The biochemical findings were in accordance with histological data, which clearly documented tissue impairment due to glycogen accumulation. Indeed, electron microscopy revealed the disruption of contractile units due to glycogen infiltrations. Furthermore, adult Agl knockout animals appeared less prompt to move, and they exhibited kyphosis. Three-mo-old Agl knockout mice could not run, and adult mice showed exercise intolerance. In addition, older affected animals exhibited an accelerated respiratory rate even at basal conditions. This observation was correlated with severe glycogen accumulation in the diaphragm. Diffuse glycogen deposition was observed in the tongues of affected mice. Our results demonstrate that this Agl knockout mouse is a reliable model for human glycogenosis type III, as it recapitulates the essential phenotypic features of the disease.

Keywords:
Glycogen storage disease type III
Metabolic disease
Glycogenosis
Glycogen debranching enzyme
Mouse model

1. Introduction

Glycogen storage disease type III (GSDIII; OMIM 232400) is an autosomal recessive disease caused by mutations in the AGL gene encoding the glycogen debranching enzyme (GDE; NP_000635.2), which catalyzes the degradation of glycogen into glucose, together with glycogen phosphorylase.

In patients with GSDIII, the liver and muscle are the major tissues involved in pathogenesis, as they normally store glycogen as a reserve. Indeed, most affected individuals lack enzyme activity in both the liver and muscle (GSDIIIa); a few (b15%) have only liver involvement (GSDIIIb), while even fewer have selective loss of one of the two catalytic activities, glucosidase (GSDIIIc) and transferase (GSDIIId) [1].

According to its clinical presentation, GSDIII is a two-phase disease. In infancy and childhood, the main symptoms are hepatomegaly starting from a few weeks/months after birth, hypoglycemia, hyperlipidemia, and growth delay [2]. These symptoms tend to decrease gradually during adolescence, although apparent glycemic control may hide progressive liver fibrosis. Cirrhosis and hepatic adenomas have also been reported, leading to hepatic transplantation in some patients [3–6]. In GSDIII patients, the onset of myopathy is now believed to occur at an earlier age than thought previously [7]; subtle motor delay in children also seems to be more frequent than previously noted. In children, the neuromuscular manifestations are hypotonia and mild weakness. In adults, myopathy is widespread (70% of patients) from the third or forth decade of life [8] and manifests as weakness in the trunk and proximal and distal muscles, with diminished grip strength and a decreased ability to jump and walk for extended times. Moreover, different muscles may show different degrees of involvement [9]. A further feature of myopathy is atrophy related to neuropathy (glycogen accumulation in peripheral nerves) and neuropathic features revealed by electromyography (EMG). Histological samples show storage of nonmembrane-bound glycogen vacuoles in the subsarcolemmal region and deep

Corresponding author at: Dino Ferrari Centre, Neuroscience Section, Department of Pathophysiology and Transplantation (DEPT), University of Milan, Neurology Unit, IRCCS Foundation Ca' Granda Ospedale Maggiore Policlinico, via F. Sforza, 35, 2022 Milan, Italy. Fax: +39 02 50320430.
E-mail address: giacomo.comi@unimi.it (G.P. Comi).
[1] These authors contributed equally to this work.

within the muscle fibers; these vacuoles can displace and ultimately replace the other cell constituents. Asymptomatic cardiomyopathy may be present as left ventricular hypertrophy in at least 50% of patients; half of these may have evolving symptoms that eventually worsen to severe cardiomyopathy [10,11].

Like other forms of glycogenosis, except for type II, treatment for patients with GSDIII seeks to control symptoms, and patients follow a suitable dietary regimen. At present, there are no fixed recommendations regarding regular exercise. This may be related to both a lack of continuous monitoring over time of strength and endurance and a lack of appropriate testing of affected individuals.

Animal disease models that replicate the major symptoms of a disease are essential to understand the disease pathogenesis and to test new drugs and therapies. Based on observations that a missense [12,13] or frameshift [14] mutation in the AGL glycogen-binding domain is enough to cause the total absence of enzyme activity, we deleted the region spanning exons 32–34 to create a constitutive knockout (KO) mouse as a disease model for GSDIII. The Agl-KO mouse presented here showed a complete absence of protein and a lack of enzymatic activity. Most importantly, it reproduced the major features of GSDIII; namely, glycogen accumulation in the liver and muscle (and thus hepatomegaly and muscle impairment), indicating that it is a reliable model for this disorder. In addition, our data highlighted aspects poorly explored previously in GSDIII patients such as central nervous system involvement and respiratory function.

2. Materials and methods

2.1. Animal studies

All procedures were approved by the Experimentation Committee of the University of Milan and were carried out in accordance with Italian guidelines for the care and use of laboratory animals. All mice were maintained in temperature- and humidity-controlled conditions, allowed free access to a standard diet of chow and water, and maintained on a 12:12 h light–dark cycle under specific pathogen-free conditions.

2.2. Generation of a constitutive Agl-KO mouse model

The KO mouse model was generated by genOway (Lyon, France). Briefly, a Neo cassette was introduced into Agl by homologous recombination in C57BL/6J embryonic stem (ES) cells, deleting exons 32–34 (the last 114 amino acids). ES cells were injected into C57BL/6J blastocysts, which were implanted into pseudopregnant females and allowed to develop to term. Southern blot analyses were performed to confirm the presence of the recombinant allele in females that resulted from this breeding. Breeders, generated by mating these heterozygotes with C57BL/6J animals, were then mated to produce the null animals.

2.3. Newborn genotyping

Genomic DNA was extracted from mouse tails with 50 mM NaOH at 100 °C for 10 min and neutralized with 3 M Tris–HCl pH 8. To determine the pattern of inheritance, two screening PCRs were designed. PCR 1 allowed for detection of Agl recombined KO alleles and was performed with a primer hybridizing downstream of the targeting vector homology sequence, with the other primer located in the Neo cassette. The expected recombined product was 1.9 kb in heterozygous and Agl-KO mice, whereas wild-type (WT) DNA yielded no amplification products. PCR 2 was performed with a primer hybridizing in the vector 3′ homology arm and a primer in a region deleted in the KO locus (exon 34). The expected endogenous product was 0.4 kb in WT and heterozygous mice. For both PCR assays, 0.2 U of Platinum Taq Polymerase (Invitrogen, Carlsbad, CA, USA) was used in a 30 μL reaction and amplification products were run on a 1.5% agarose gel.

2.4. Biochemical assays

Mice were sacrificed by cervical dislocation. Tissues for analysis were then rapidly excised, frozen in liquid nitrogen, and stored at −80 °C.

2.4.1. Western blot analysis

Homogenized extracts (20 μg of protein) from the skeletal muscle, brain, liver, and heart tissue of WT, heterozygous, and KO mice were analyzed. The protein extract was separated on a 6% acrylamide gel and electrophoretically transferred to a nitrocellulose membrane. The blots were probed for expression of GDE with rabbit polyclonal antibody (1:2200; Agrisera, Vannas, Sweden) and peroxidase-conjugated secondary antibody. The signal was detected with an ECL detection kit (Amersham-GE Healthcare, Little Chalfont, UK).

2.4.2. GDE activity

Debrancher enzyme activity was measured in frozen muscle and liver tissue with an indirect assay based on stimulation of the incorporation of radioactive glucose into glycogen [15]. Enzyme activity was expressed as picomoles of glucose incorporated into glycogen/min/mg protein.

2.4.3. Determination of glycogen absorption spectrum and content

The absorption spectrum of glycogen was evaluated by the glycogen–iodine complex method [16]. Amyloglucosidase digestion of ethanol-precipitated glycogen was used to assess the glycogen content from the skeletal muscle, liver, heart, and brain (20–70 mg of tissue) samples, as previously described [17]. We increased the amyloglucosidase working concentration up to 0.6 mg/ml. After amyloglucosidase digestion, we estimated glucose concentration in diluted samples with the Glucose Hexokinase Kit (Greiner Diagnostic, Bahlingen, Germany). Absorbance was read at 340 nm after a 5 min incubation at 37 °C.

2.5. Laboratory testing

2.5.1. Glycemia

Glycemia values were measured with blood glucose test strips in a FreeStyle Optium H system (Abbott Diabetes Care, Witney, UK). Tail vein blood samples were collected from 7- and 8-mo-old mice.

2.5.2. Serum biochemistry

Blood samples were collected by intracardiac puncture after anesthesia. This procedure was followed by euthanasia. Blood was gathered in tubes and centrifuged at 3000 rpm for 5 min to collect serum. Serum was frozen and sent to Charles River Laboratories to be analyzed.

2.6. Histology and electron microscopy

For light microscopy studies, fresh organs and tissues were immediately frozen in isopentane, cooled in liquid nitrogen, and then processed according to standard methods [18]. Routine stains with and without prior diastase digestion were performed with hematoxylin and eosin, Gomori Trichrome (TG), Masson, and periodic acid–Schiff (PAS). Semithin sections, stained with toluidine blue, were examined by light microscopy. For ultrastructural examination, muscle samples were fixed in 2.5% glutaraldehyde (pH 7.4) and postfixed in 2% osmium tetroxide. After dehydration in a graded series of ethanol concentrations, the samples were embedded in Spurr's resin. Finally, ultrathin sections were examined with a Zeiss EM109 transmission electron microscope [18].

2.7. Evaluation of muscle performance

All animals were tested in the morning during the light phase of the light–dark cycle. Isolated mice and pregnant females were excluded.

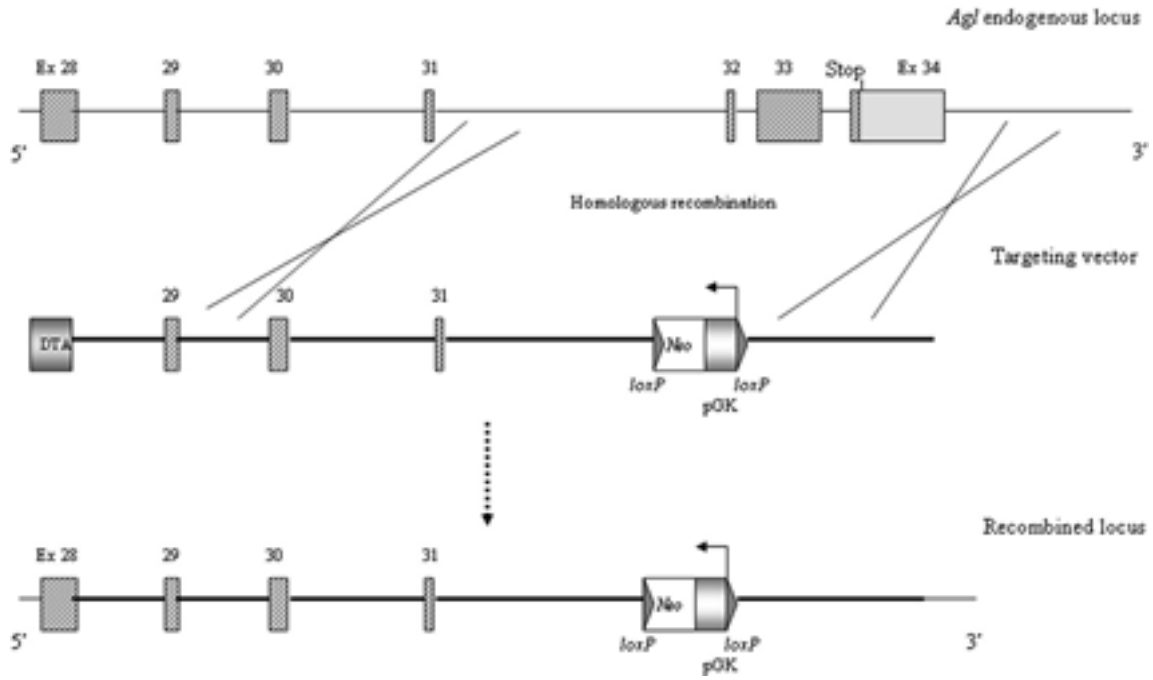

Fig. 1. Targeted disruption of the Agl gene. Schematic representation of the targeting vector and the homologous recombination product.

2.7.1. Hind print test

The footprint test was used to compare the gait of the Agl-KO mice with that of their WT counterparts. For the hind print test, nontoxic paint was applied to the inside of the hind paws of the mice. They were then placed on a paper sheet at the beginning of a corridor (10 cm × 60 cm) and allowed to complete the maximum length achievable.

2.7.2. Treadmill test

Mice were trained for 2 days on a single lane treadmill (Panlab LE8708; Panlab Harvard Apparatus, Cornellà, Spain) supplied with an electrified grid to provide motivation with a mild shock (0.2 mA). The incline was 5° with an accelerating speed from 5 to 15 cm/s during 15 min. Mice were administered two different experimental conditions after a warming run of 3 min on a speed belt at 10 cm/s. For the first protocol, animals were run at 30 cm/s for 5 min. For the second, mice were tested at a constant belt speed of 15 cm/s and allowed to cover a maximum distance of 350 m. For both experiments, the incline was 5°. The tests were interrupted when the mouse was unable to remain on the belt.

2.7.3. Rota-rod test

The Rota-rod (Accelerating Model; Ugo Basile, Varese, Italy) was used to measure forelimb and hindlimb motor coordination and balance. Before the test, mice were trained by undergoing one trial per day for two consecutive days. For the rota-rod test, mice were placed on a rotating rod accelerating from 5 to 20 rpm in 5 min. Each mouse was tested twice; the best performance from each mouse was considered, and the results were expressed as mean ± standard deviation (SD).

2.8. Statistical analysis

The Kaplan–Meier estimator was employed to plot lifetime data and calculate the survival function. Statistical significance was estimated with Student's t-test to compare experimental groups. Error bars denote SD. A P value of $b0.05$ was considered statistically significant.

3. Results

3.1. Generation and general features of Agl-KO mice

Agl-KO mice were created by deletion of the carboxy terminus of GDE, including the glucosidase and glycogen-binding domains (Fig. 1). The affected mice were viable, but presented higher mortality in adulthood than WT mice (Fig. 2A), whereas heterozygotes were viable and fertile and did not show any differences compared to WT animals. Agl-KO mice did not differ considerably in size or appearance from their WT and heterozygous littermates at birth or during development (Fig. 2B).

Western blot analysis of the skeletal muscle, heart, liver, and brain tissue confirmed the total absence of GDE in all tissues from Agl-KO mice (Fig. 2C). In heterozygotes, GDE protein was significantly reduced compared to WT. As expected, GDE activity was almost null in Agl-KO mice (skeletal muscle, 2.30 ± 1.25 and liver, 5.58 ± 1.65 pmol glucose/min/mg protein; n = 3) compared to WT mice (skeletal muscle, 216.25 ± 36.40 and liver, 37.23 ± 1.45 pmol glucose/min/mg protein; n = 3). Heterozygotes exhibited lower GDE activity (skeletal muscle, 134.23 ± 13.51 and liver, 23.37 ± 6.34 pmol glucose/min/mg protein; n = 3) than WT mice (Table 1).

Upon autopsy, macroscopic examination revealed that Agl-KO livers were enlarged and dark red in color compared to WT liver (Fig. 2E). We did not observe nodules indicating cirrhosis or adenomas, even at advanced age (18 mo; n = 1). Livers from 3-mo-old Agl-KO mice had increased to over 9% of total body weight and up to 11% in mice aged 12 mo, whereas the liver comprised between 5 and 6% of total body weight in WT mice (n = 4 for each group) (Fig. 2D). No differences were observed in the dimensions or percent of total body weight of the heart between Agl-KO and WT mice at any age (n = 4 for each group) (Suppl. Fig. 1).

3.2. Glycogen content

Absorbance spectrum measurements of liver glycogen revealed an absence of the 460-nm peak, as observed in GSDIII patients; this indicates an abnormal glycogen structure (i.e., phosphorylase-limit dextrin)

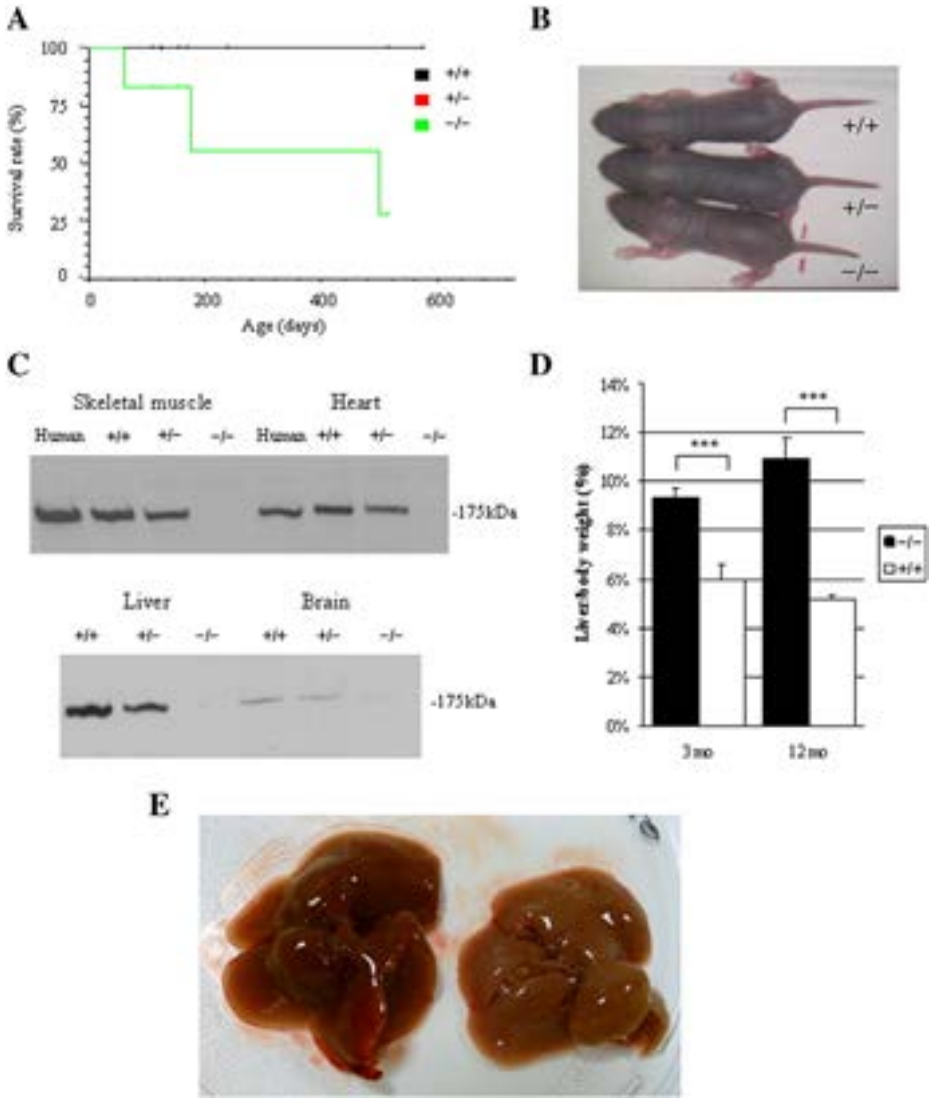

Fig. 2. Characterization of Agl-KO mice. A) Kaplan–Meier curve. Lines representing survival of heterozygous and WT mice are superimposed (n = 10 for each group). B) Photograph of 4-d-old mice. No appreciable differences in general appearance were noted among genotypes. C) Western blot demonstrating the absence of GDE protein in all tissues from Agl-KO mice. D) Liver weight expressed as percentage of whole body weight in WT and Agl-KO mice at 3 and 12 mo of age (n = 4 for each group). E) Agl-KO liver appeared enlarged and dark red in color compared to WT liver. Signs of cirrhosis or adenomas were not observed. ***P b 0.0001. Means ± SD are shown.

(Fig. 3A). Differences in peak width accounted for different glycogen amounts among samples.

We next assessed glycogen content in the skeletal muscle, liver, heart, and brain tissue from adult Agl-KO, heterozygous, and WT mice (n = 5 for each group, except for the heart: n = 3). All affected tissues contained substantial amounts of glycogen (skeletal muscle, 4.5 ± 0.9; liver, 7.7 ± 0.6; heart, 2.1 ± 0.3; and brain, 0.2 ± 0.04 g/100 g tissue), which were higher than in heterozygous (skeletal muscle, 0.3 ± 0.05; liver, 2.7 ± 0.7; heart, 0.01 ± 0.01; and brain, 0.01 ± 0.01 g/100 g tissue) and WT (skeletal muscle, 0.2 ± 0.07; liver, 2.9 ± 1.1; and heart, 0.08 ± 0.0.07 g/100 g tissue; brain, glycogen not detectable) tissues (Fig. 3B). All P values b 0.0005.

Table 1
GDE activity in skeletal muscle and liver.

	GDE activity pmol glucose/min/mg protein		
	+/+	+/−	−/−
Skeletal muscle (n = 3)	216.25 ± 36.40	134.23 ± 13.51	2.30 ± 1.25
Liver (n = 3)	37.23 ± 1.45	23.37 ± 6.34	5.58 ± 1.65

3.3. Glycemia

Adult fed Agl-KO mice had basal blood glucose values significantly lower (92 ± 9 mg/dl; n = 5) than heterozygous (132 ± 9 mg/dl; n = 5) and WT (164 ± 18 mg/dl; n = 5) mice (Agl-KO vs. WT mice, P b 0.0001) (Fig. 4). After 16 h of fasting, glycemia was considerably reduced in Agl-KO mice (59 ± 8 mg/dl; n = 4) compared to heterozygous and WT mice (111 ± 17 mg/dl and 100 ± 21 mg/dl, respectively; n = 4 for each) (Fig. 4A).

3.4. Serum biochemistry

Serum biochemistry (Fig. 4B) in Agl-KO fed mice revealed high levels (1.8–12.6 fold) of ALT, AST and ALP in 3-mo-old (AST 223 ± 126 U/l; ALT 95 ± 55 U/l; ALP 96 ± 10 U/l) and in 12-mo-old mice (AST 469 ± 105 U/l; ALT 146 ± 44 U/l; ALP 91 ± 23 U/l) compared to WT mice (3-mo: AST

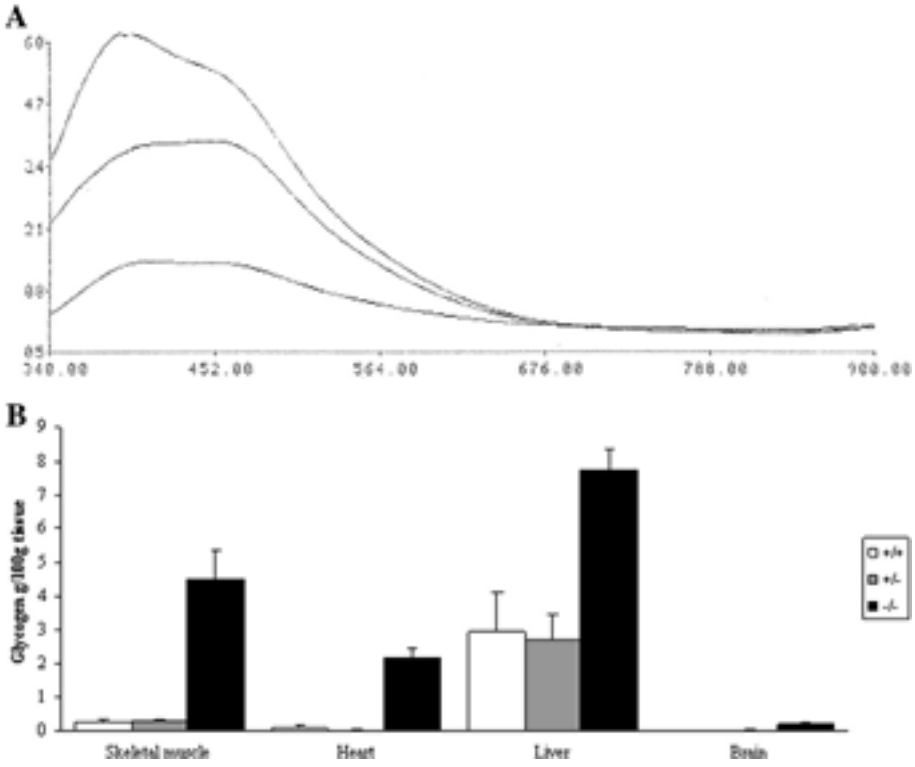

Fig. 3. Glycogen content. A) Absorbance spectrum showing abnormal glycogen structure and content in 4-mo-old Agl-KO mice. B) Histogram depicting increased glycogen content in all tissues from Agl-KO mice (n = 5 for each group except the heart n = 3). All of P values b0.0005. Means ± SD are shown.

64 ± 35 U/l; ALT 46 ± 16 U/l; ALP 41 ± 9 U/l; 12-mo: AST 37 ± 5 U/l; ALT 24 ± 5 U/l; ALP 49 ± 14 U/l). Liver transaminases increased with age, whereas ALP remained steadily higher. Examination of serum triglycerides (TRIG) and total cholesterol (CHOL) did not show any difference between Agl-KO (3-mo: TRIG 79 ± 35 mg/dl; CHOL 81 ± 9 mg/dl; 12-mo: TRIG 86 ± 31 mg/dl; CHOL 83 ± 13 mg/dl) and WT mice (3-mo: TRIG 100 ± 20 mg/dl; CHOL 84 ± 7 mg/dl; 12-mo: TRIG 74 ± 37 mg/dl; CHOL 84 ± 8 mg/dl) not even at old ages. Serum CK was significantly higher in Agl-KO (3-mo: 247 ± 57 mg/dl; 12-mo: 272 ± 53) than in WT mice (3-mo: 87 ± 6 mg/dl; 12-mo: 43 ± 11 mg/dl) at both young and old ages (P b 0.05).

3.5. Histology and electron microscopy

We performed a detailed histological examination of the liver, muscle, heart, brain, cerebellum and sciatic nerve from 4-, 8-, 12-, and 18-mo-old mice. Significant glycogen accumulation was detected in skeletal muscle (vastus, Fig. 5B–E), and in hepatocytes from Agl-KO mice at all ages (Fig. 5G–L), while heterozygous mice did not show any changes compared to their respective WT littermates (data not shown). In Agl-KO mice, hepatocytes appeared enlarged due to glycogen deposition. However, the liver did not exhibit fibrosis (Fig. 6) even in older mice, and there was no evidence of inflammation at any age. Glycogen deposition in cardiac tissue was found in Agl-KO mice at all examined ages (Fig. 5N–Q). TG analysis revealed that pathological alterations were present in all of the muscles tested from Agl-KO mice: vastus, gastrocnemius, and diaphragm (Fig. 7).

Ultrastructural examination (Fig. 8) of skeletal muscle from 4- and 12-mo-old mice reflected the histological findings that assessed muscle damage in Agl-KO mice. In muscle tissue from 4-mo-old affected animals, we found glycogen granules dispersed among the myofibrils (Fig. 8A). In 12-mo-old Agl-KO mice, muscle fibers contained large glycogen collections that were localized both at the subsarcolemmal level and at intracytoplasmic sites. Large regions of the sarcoplasm were entirely occupied by cytoplasmic glycogen, leading to marked alterations in the muscle architecture (Fig. 8B).

We did not find any morphological alterations in the brain or cerebellum with respect to WT mice. However, PAS staining showed a slight increase of glycogen content in brain frontal cortex in all Agl-KO mice examined (Fig. 9). Furthermore, in cerebellum we observed PAS-positive glycogen deposits in the granular layer adjacent to the Purkinje cell layer (Fig. 9) which increased with age; the highest amounts of glycogen were observed in 18-mo-old Agl-KO mice.

We analyzed sciatic nerve in 12- and 18-mo-old Agl-KO mice by light microscopy. As shown in Supplementary Fig. 2, nerve tissue had a normal appearance and no glycogen granules were detected.

Since a recent clinical study observed fatty infiltration in the tongue musculature in some GSDIII patients [19], we analyzed tongue tissue from 4- and 18-mo-old mice. In Agl-KO mice, we found glycogen accumulation, as shown in Supplementary Fig. 3.

3.6. Evaluation of muscle performance

Adult Agl-KO mice appeared to be slower than their littermates, and the hind print test showed everted paws during walking, even in 3-mo-old Agl-KO mice, suggesting early muscle involvement (Fig. 10A). To further assess muscle performance in young mice, we first evaluated their ability to run on a treadmill device using a belt speed of 30 cm/s. We tested 4 Agl-KO mice and observed significant performance variability. Indeed, at 2 mo of age, 2 mice were able to run for the maximum time established (5 min), whereas 2 mice could only run for a few seconds. The same mice tested at 3 months of age showed a dramatic decrease of their performances: those that performed better in the first test could run just half a minute in the second, whereas the other ones were not able to remain on the belt (Fig. 10B). We then tested 9-mo-old mice (n = 5 for each group). None of the Agl-KO mice were able to remain on the belt, whereas WT mice were able to run for 5 min.

We next assessed the capacity of the mice to perform mild exercise for long distances (belt speed of 15 cm/s for 350 m). Under these

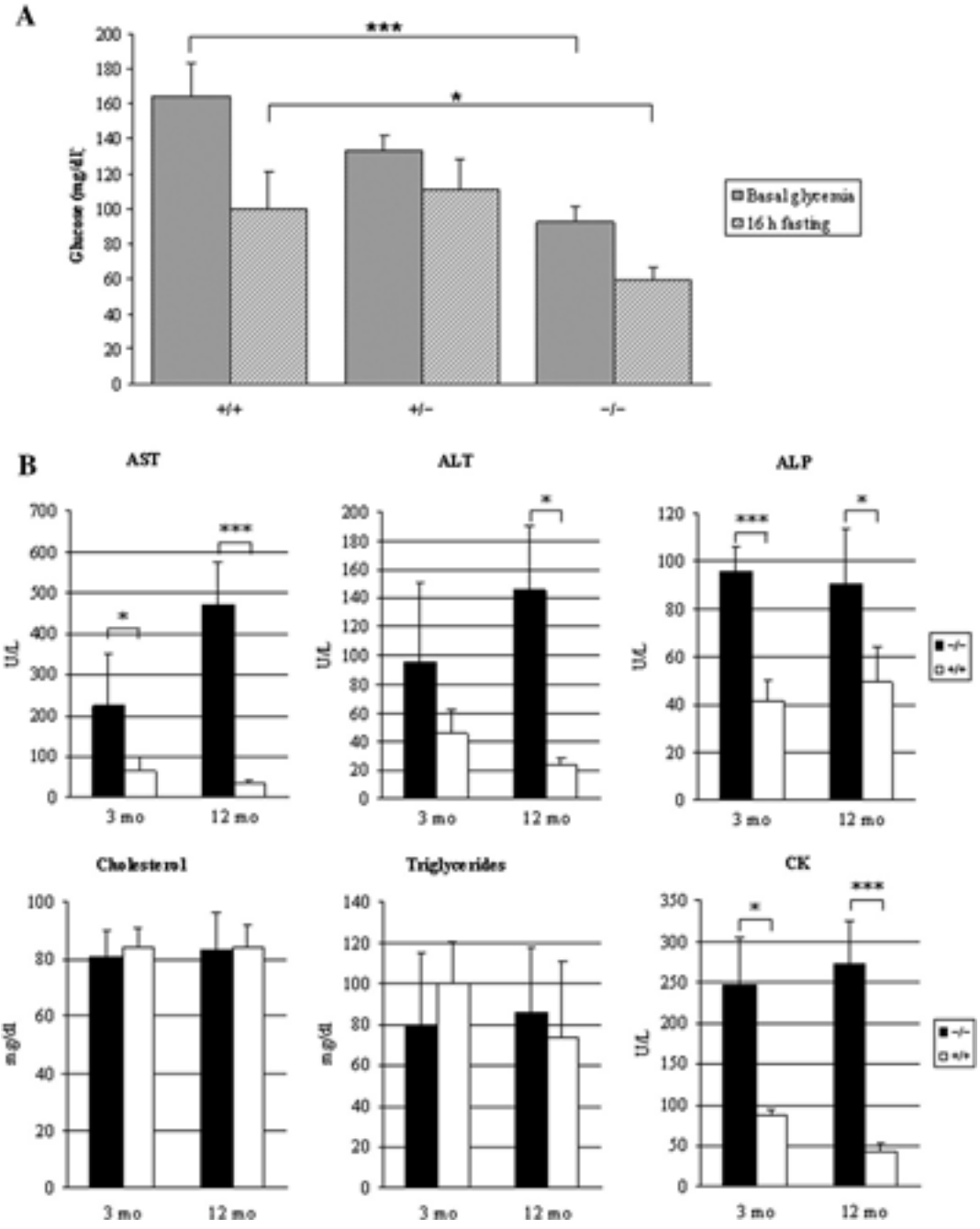

Fig. 4. Biochemistry detection. A) Blood glucose determination in 7 and 8 mo aged mice. Basal glycemia in Agl-KO mice was significantly lower than in heterozygous and WT mice (gray bars; n = 5). As expected, after 16 h fasting, blood glucose levels decreased in all genotypes; nevertheless, glucose values were still significantly different between Agl-KO and WT mice (lined bars; n = 4). ***P b 0.0001, *P b 0.05. B) Serum biochemistry in Agl-KO and WT fed mice at 3 and 12 mo of age. ***P b 0.005, *P b 0.05 Means ± SD are shown.

conditions, Agl-KO mice were able to remain on the belt and execute the test. One of the mice reached 350 m. Agl-KO mice walked for a mean distance of 228 ± 80 m, while WT mice walked for 350 m (P b 0.05) (Fig. 10C).

Motor coordination was evaluated by Rota-rod test. In an accelerating test (from 5 to 20 rpm in 5 min), 8-mo-old Agl-KO mice performed less well than age-matched controls (P b 0.05; n = 8 for each group). Only two out of eight Agl-KO mice were able to complete the test (Fig. 10D).

4. Discussion

GSDIII is a rare genetic metabolic disorder that mainly affects the liver, skeletal muscle and heart. This glycogenosis is incurable, and a suitable dietary is the only treatment currently available. Here we describe a constitutive KO mouse model obtained by deleting the last 114 amino acids of the debranching enzyme. A natural canine model of GSDIII has been reported [14], in which the loss of GDE is caused by a deletion of the last 126 amino acids due to a frameshift mutation. Another model for GSDIII was published recently by Liu and colleagues [20]: a KO mouse generated by disrupting the Agl gene downstream of exon 5.

Viability data collected for our Agl-KO mice suggested a tendency toward a higher mortality within 1 y of age compared to WT mice (Fig. 2A). Viability data presented here are similar to those described for the other GSDIII KO mouse model. No mortality is reported in the dog model. Mortality has never been reported in GSDIII patients [9], but large longitudinal studies are lacking. While human diets are

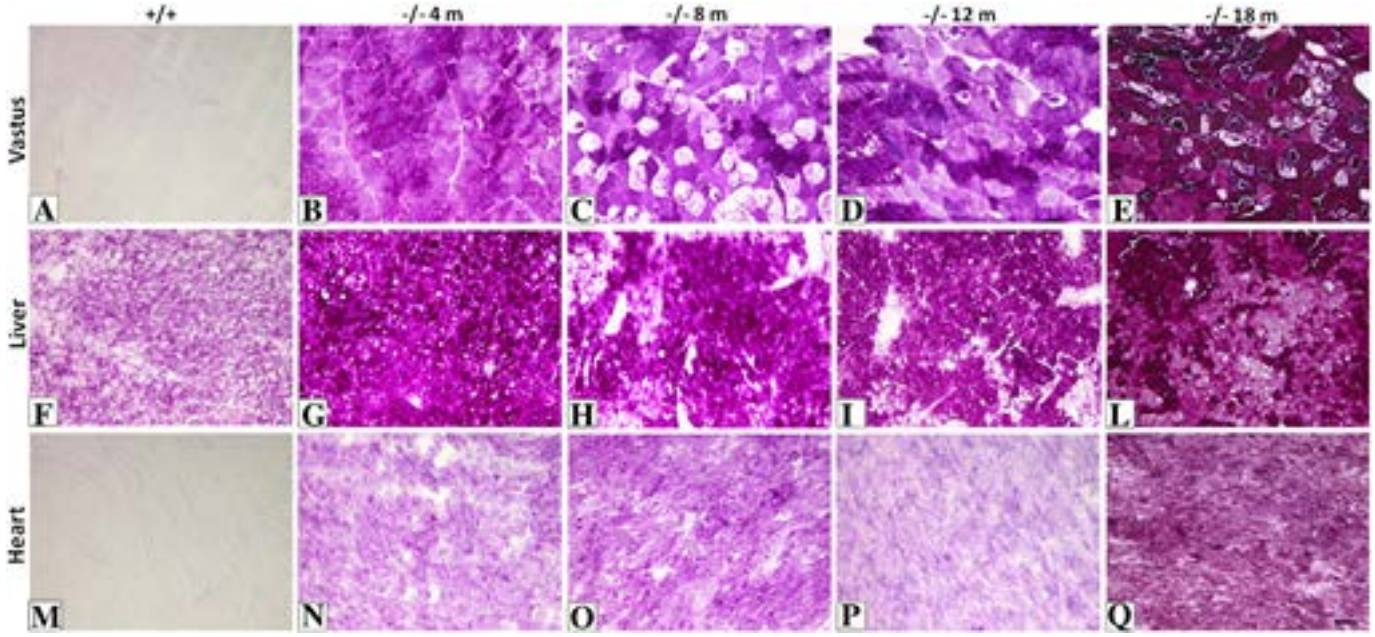

Fig. 5. PAS staining showing glycogen accumulation in Agl-KO mice. WT mice (A, F, M); 4-mo-old (B, G, N), 8-mo-old (C, H, O), 12-mo-old (D, I, P), and 18-mo-old (E, L, Q) Agl-KO mice. Vastus (A–E), liver (F–L), and heart (M–Q). Scale bar: 20 μm.

modified to treat GSDIII, for our animal model, no dietary correction was provided. In addition, Agl-KO mice exhibited a severe muscle impairment that could prevent the most affected animals from adequately feeding.

No growth delay was ascertained in the affected mice, which is in accordance with observations in other GSDIII models [20,21], but in contrast to a clinical feature frequently reported in patients [22,23].

When we examined the liver tissue from mice sacrificed at different ages, we did not notice signs of cirrhosis or adenomas in the Agl-KO mice, even in one 18-mo-old animal. Nevertheless, these mice presented hepatomegaly, and liver parenchyma appeared darker compared to WT (Fig. 2D and E). Marked amounts of glycogen storage were observed starting at young ages in affected liver cells, which appeared enlarged (Figs. 5 and 6). As shown in Fig. 6, there was no evidence of inflammation or fibrosis in the liver, even in older mice. In both previously reported GSDIII animal models, signs of liver fibrosis were described; in the curly-coated retrievers, diffuse nodular cirrhosis was also observed.

We observed that basal glycemic values were lower in adult Agl-KO mice compared to their WT and heterozygous littermates. The physiological lack of debranching enzyme in this disease leads to reduced glucose levels if no corrections are made to carbohydrate dietary intake. Our mouse model was fed a standard diet, and this may explain the lower basal levels of glucose in the affected mice. Other experiments are needed to elucidate the complex metabolic features underlying this pathological condition.

Serum biochemistry parameters on normally fed Agl-KO mice reflected the main pathological features found in human patients and were in agreement with histological and functional findings. Hyperlipidemia, which is frequently found in human patients, was not observed

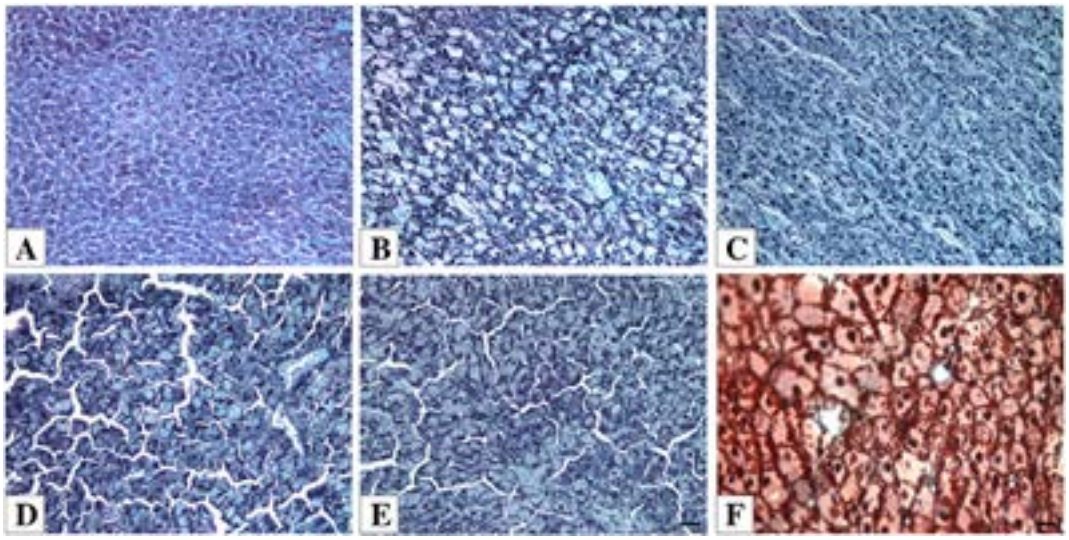

Fig. 6. Gomori trichrome and Masson's staining of liver tissue. WT mouse (A); 4-mo-old (B), 8-mo-old (C), 12-mo-old (D) and 18-mo-old Agl-KO mice (E, F). TG staining: A–B–C–D–E. Masson's staining: F. Scale bar (A, B, C, D, E): 25 μm. Scale bar (F): 12.5 μm.

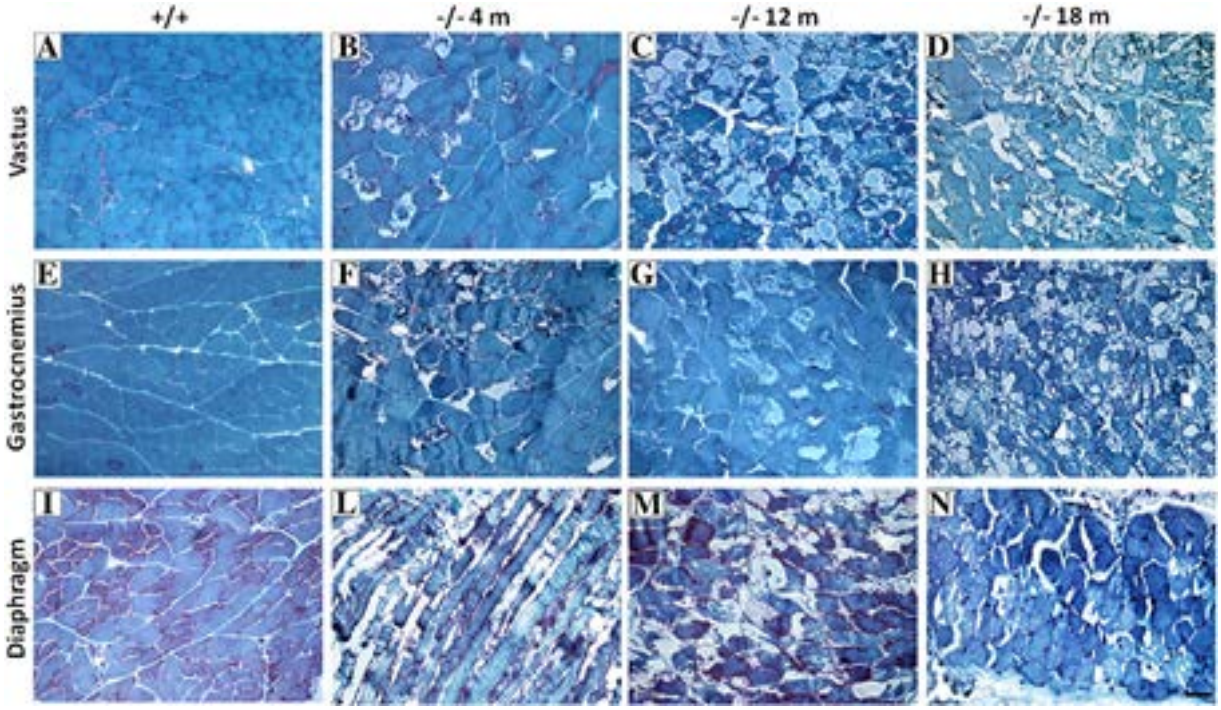

Fig. 7. Representative light microscopy images showing progressive muscle fiber vacuolization. WT mice (A, E, I); 4-mo-old (B, F, L), 12-mo-old (C, G, M), and 18-mo-old (D, H, N) Agl-KO mice. Vastus (A–D), gastrocnemius (E–H), and diaphragm (I–N). Scale bar: 20 μm.

in our animal model (Fig. 4B). Indeed, triglyceride and cholesterol levels were normal in both dog and mouse models previously reported [20, 21]. Serum AST, ALT and ALP were considerably increased in young mice and significantly higher than WT in older mice (12.6, 6.1 and 1.8 fold). These data were a further confirmation of liver damage due to abnormal glycogen storage clearly demonstrated by histological analysis (Figs. 5 and 6) and correlated with high transaminase levels found in GSDIII patients. Similarly, CK levels were significantly higher in Agl-KO mice even at 3 mo of age. Liu and colleagues reported normal CK values, whereas GSDIIIa dog showed CK increase beginning at 10 mo

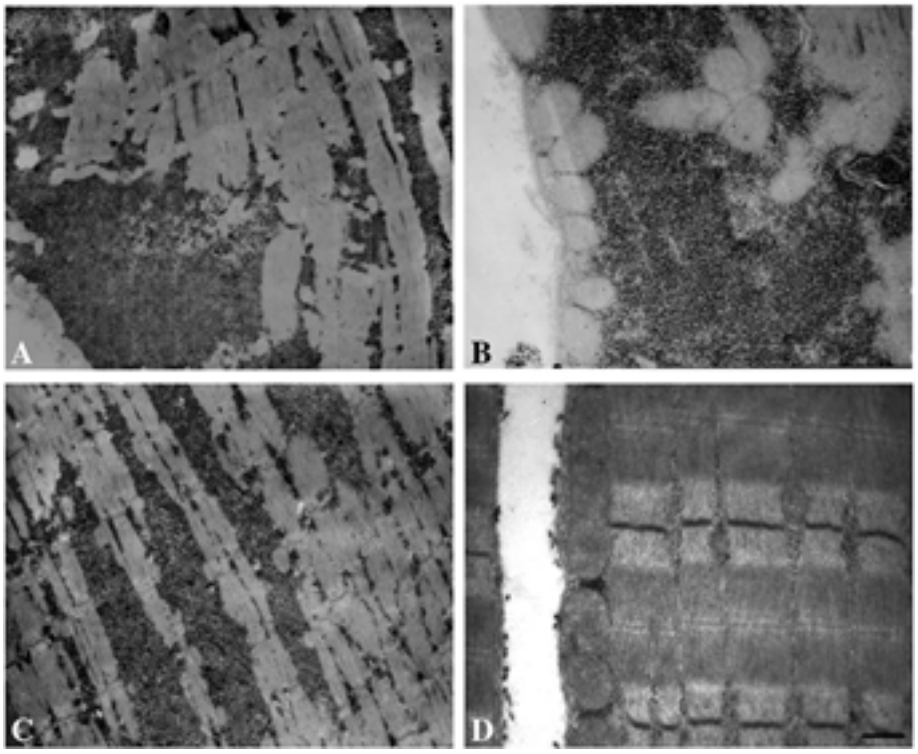

Fig. 8. Ultrastructural analysis. Representative electron microscopic images of 4-mo-old Agl-KO mice (A), 12-mo-old Agl-KO mice (B), 12-mo-old heterozygous mice (C), and WT mice (D). In 4-mo-old Agl-KO mice (A), glycogen granules were dispersed among the myofibrils. In 12-mo-old Agl-KO mice (B), large glycogen collections were localized at the subsarcolemmal level and at intracytoplasmic sites. Large regions of the sarcoplasm were entirely occupied by cytoplasmic glycogen, leading to marked alterations in muscle architecture. Scale bars: 1428 nm (A, C) and 833 nm (B, D).

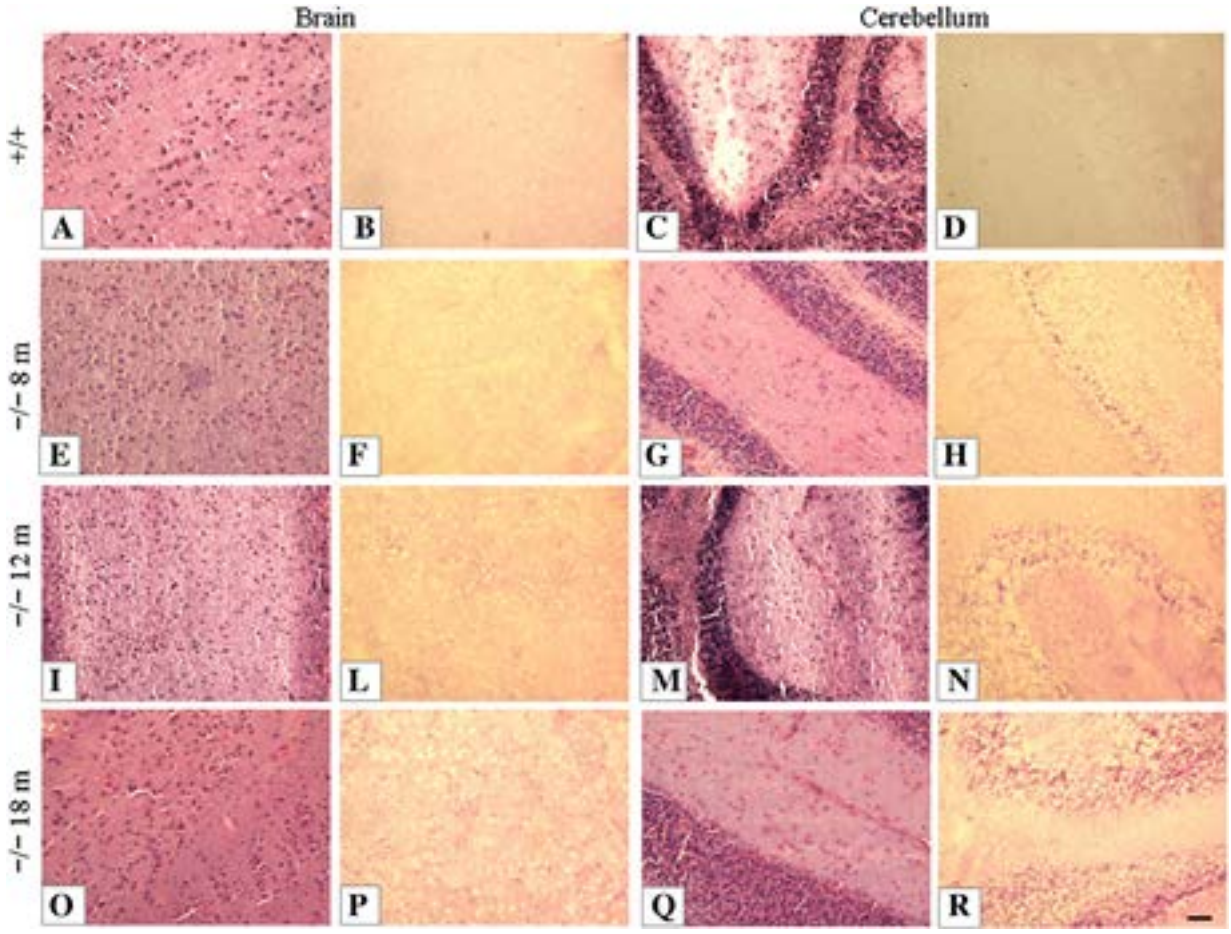

Fig. 9. Representative light microscopy images showing a light glycogen increase in the brain and cerebellum. WT mice (A, B, C, D); 8-mo-old (E, F, G, H), 12-mo-old (I, L, M, N) and 18-mo-old Agl-KO mice (O, P, Q, R). Brain (A, B, E, F, I, L, O, P), cerebellum (C, D, G, H, M, N, Q, R). A–E–I–O–C–G–M–Q: Hematoxylin–eosin staining. B–F–L–P–D–H–N–R: PAS staining. Scale bar: 25 μm.

of age. In our model, Agl-KO mice expressed muscle phenotype starting at a young age (Fig. 10). In addition, GSDIII patients have been previously reported to have increased CK levels since the first decade of life [24].

The glycogen content (Fig. 3B) was significantly higher in all of the tissues predominantly affected by the disease. Marked glycogen deposition was noticed in the heart from Agl-KO mice, but these mice did not develop fiber hypertrophy or fiber disarray (Suppl. Fig. 1B). The heart/body weight ratio did not suggest cardiac hypertrophy (Suppl. Fig. 1A). We cannot exclude cardiomyopathy, though it was not reported in the mouse model by Liu and colleagues who performed echocardiography analysis [20]. Left ventricular hypertrophy is common in GSDIII patients, although a limited number of patients actually develop symptomatic cardiomyopathy [9,10].

With respect to musculoskeletal involvement, adult Agl-KO mice were less prompt to move and slower than their healthy littermates. Furthermore, adult mice exhibited kyphosis. This fact, together with the decreased muscular performance and a gait defect (everted paws), may be related to the diminished capacity of affected mice to stay coordinated on the Rota-rod device. Postural defects, such as mild lumbar lordosis, which presumably occurs to accommodate increased abdominal girth due to hepatomegaly, have been reported in some adult patients with GSDIII [9].

Muscle tissues of Agl-KO mice showed a dramatic increase in the glycogen amount which was 20-fold higher than in WT muscles (Fig. 3B). The biochemical findings were in accordance with histological data (Fig. 5). TG confirmed the progressive alteration of muscle macroscopic architecture (Fig. 7), and electron microscopy (Fig. 8) revealed that the structure of the functional units was altered due to glycogen infiltrations. Indeed, 2- and 3-mo-old mice forced to run at 30 cm/s showed early and unexpected muscle impairment. Nine-mo-old Agl-KO mice could not run at all. Furthermore, when adult Agl-KO mice were tested with mild exercise on the treadmill, their performance was worse than healthy mice, although one Agl-KO animal was able to complete the exercise (Fig. 10). The exercise intolerance observed in adult Agl-KO mice is likely due to muscle wasting, but we cannot exclude that it may also arise from metabolic derangement, as suggested in a recent study by Preisler et al. [25]. These authors diverged from the conventional notion that muscle wasting is primarily responsible for fixed weakness and suggested that the muscular symptoms in GSDIII are related to dynamic exercise; that is, they may be associated with impaired muscle glycogenolysis.

Glycogen accumulation in GSDIIIa dogs produced progressive damage in muscle, with disruption of the contractile apparatus from 12 mo of age. The mouse model by Liu and colleagues showed signs of muscle weakness and decreased muscle strength at 1 y of age associated with normal CK values.

In order to better characterize the localization of glycogen in central and peripheral nervous systems in Agl-KO mice, we performed a histological analysis of brain and cerebellum at different ages. We did not find any morphological alteration in both tissues with respect to WT mice. However, in all Agl-KO mice examined PAS staining showed a slight increase of glycogen in brain frontal cortex. In cerebellum, mild

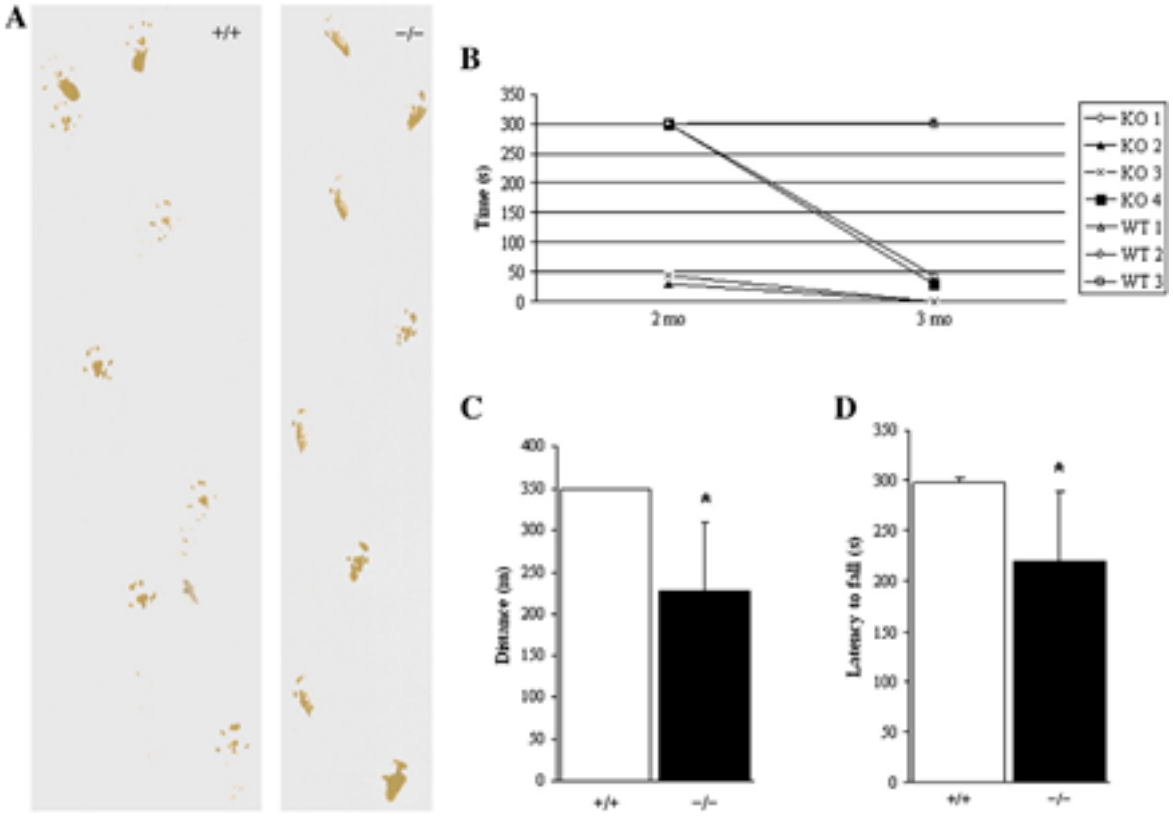

Fig. 10. Functional assessment of muscle performance. A) Hind print test. 3-mo-old Agl-KO mice showed a gait defect compared to healthy littermates. B) Running test on 2- and 3-mo-old mice with speed belt of 30 cm/s. At 3 mo of age running ability was dramatically impaired (Agl-KO n = 4; WT n = 3). C) Treadmill test showed that at low speed (15 cm/s), Agl-KO mice were able to run on the belt, although they covered short distances (n = 5). D) In the Rota-rod test, 8-mo-old Agl-KO mice showed less-coordinated movements and were more prompt to fall (n = 8). *P b 0.05. Means ± SD are shown.

PAS-positive glycogen deposits were revealed in the granular layer just adjacent to the Purkinje cells, especially evident in 18-mo-old mice (Fig. 9). Because the cerebellum is responsible for proper muscle tone and equilibrium we hypothesize that defective coordination revealed by Rota-rod test might be related to glycogen deposits in granular layer. No studies on nervous system have been described on the other GSDIII models. Peripheral neuropathy has been reported in few patients due to glycogen accumulation in peripheral nerves [26,27]. However, morphological alteration due to glycogen storage was not detected in sciatic nerve from 12- and 18-mo-old Agl-KO mice (Suppl. Fig. 2).

As a further pathological feature of our mouse model, we noticed an accelerated respiratory rate in older animals compared to heterozygous and WT littermates, even at basal conditions. This observation correlated with the severe glycogen accumulation observed in the diaphragm (Fig. 7L–N) of a 12-mo-old mouse with respiratory impairment. Patients with generalized myopathy tend to have more severe weakness that often affects the respiratory muscles [23,28].

Histological analysis of tongue tissue from affected mice revealed diffuse glycogen deposition in the intrinsic musculature (Suppl. Fig. 3). Infiltration of glycogen in the tongue was described in the canine model of GSDIII [21] and in some patients, in whom it may be associated with speech and language pathology and dysphagia [19].

The results presented here regarding our Agl-KO mouse model suggest that it is a reliable model for GSDIII, since it exhibits the essential phenotypic features of this disease in humans, such as liver and muscle impairment. In our mouse model, marked muscle impairment was clearly detectable starting at 2 mo of age, whereas the mouse model described by Liu and colleagues seemed to exhibit reduced motor activity at 1 y of age. Furthermore, our data indicate a possible and not yet reported involvement of central nervous system that could be worth for deep investigation in GSDIII patients. We believe that this model will be of use in future studies of GSDIII pathophysiology, as well as for testing new treatments and therapies.

Supplementary data to this article can be found online at http://dx.doi.org/10.1016/j.bbadis.2014.07.029.

Conflict of interest

None of the authors have any conflicts of interest to declare.

Acknowledgements

We are grateful to the Italian Association for Glycogenosis (AIG), which provided critical financial support for this work. We thank Dr. Fabrizio Seidita for his continuing support. We also thank the ONG Foundation "Associazione Amici del Centro Dino Ferrari" for its long-term assistance and the Italian Association of Myology (AIM). Many thanks to Dr. Carolyn Ritterson Lew for her help in manuscript revision.